ARTICLE

Reinforcing Poly(ε-caprolactone) Nanofibers with Cellulose Nanocrystals

Justin O. Zoppe,[†] Maria S. Peresin,[†] Youssef Habibi,[†] Richard A. Venditti,[†] and Orlando J. Rojas*[,†,‡]

Department of Forest Biomaterials, North Carolina State University, Raleigh, North Carolina 27695-8005, and Department of Forest Products Technology, Faculty of Chemistry and Materials Sciences, Helsinki University of Technology, P.O. Box 3320, FIN-02015 TKK, Finland

ABSTRACT We studied the use of cellulose nanocrystals (CNXs) obtained after acid hydrolysis of ramie cellulose fibers to reinforce poly(ε-caprolactone) (PCL) nanofibers. Chemical grafting with low-molecular-weight PCL diol onto the CNXs was carried out in an attempt to improve the interfacial adhesion with the fiber matrix. Grafting was confirmed via infrared spectroscopy and thermogravimetric analyses. The polymer matrix consisted of electrospun nanofibers that were collected as nonwoven webs. The morphology as well as thermal and mechanical properties of filled and unfilled nanofibers were elucidated by scanning electron microscopy, differential scanning calorimetry, and dynamic mechanical analysis, respectively. The addition of CNXs into PCL produced minimal changes in the thermal behavior of the electrospun fibers. However, a significant improvement in the mechanical properties of the nanofibers after reinforcement with unmodified CNXs was confirmed. Fiber webs from PCL reinforced with 2.5% unmodified CNXs showed ca. 1.5-fold increase in Young's modulus and the ultimate strength compared to PCL webs. Compared to the case of grafted nanocrystals, the unmodified ones imparted better morphological homogeneity to the nanofibrillar structure. The grafted nanocrystals had a negative effect on the morphology of nonwoven webs in which individual nanofibers became annealed during the electrospinning process and, therefore, could not be compared to neat PCL nonwoven webs. A rationalization for the different effects of grafted and unmodified CNXs in reinforcing PCL nanofibers is provided.

KEYWORDS: cellulose nanocrystals • nanocrystalline cellulose • cellulose whiskers • surface grafting • electrospinning • fiber reinforcement • nanofibers • nanocomposites • nanoparticles • poly(ε-caprolactone)

INTRODUCTION

The manufacture and use of nanofiber-based scaffolds have recently attracted interest in biomedical applications, especially for tissue engineering (1−6). One of the main goals in this area is to create biocompatible and biodegradable scaffolds with mechanical and biological properties similar to those of extracellular matrixes (ECMs) so as to facilitate surgical implants and promote tissue regeneration (7). Natural and synthetic polymers have been examined for this purpose, including collagens, chitosan, hyaluronic acid, and biodegradable polyesters such as poly(lactic acid), poly(glycolic acid), and polycaprolactone, among others. Synthetic, biodegradable poly(ε-caprolactone), or PCL, has been shown to be particularly useful when used in the production of electrospun fibers to mimic ECMs (8−10). However, there are a few challenges that need to be overcome in the application of PCL, including effects brought about by its hydrophobicity, which can potentially prevent living cell adhesion and mobility and also limit mechanical strength (required to ensure structural integrity) (11). In order to reduce its surface energy, PCL is usually blended with hydrophilic polymers, thereby facilitating cell adhesion (5). On the other hand, improvement of the mechanical and thermal properties of PCL-based scaffolds can be accomplished by reinforcing them with suitable fillers (12).

Recently, efforts to increase the mechanical properties of PCL nanofiber webs have been reported by the addition of carbon nanotubes (CNTs) (13, 14). Although the introduction of CNTs yielded composite fibers with increased mechanical properties, manufacture protocols required demanding processing conditions (15); therefore, it is anticipated that such types of composites can be quite costly. In addition, CNTs possess some degree of toxicity (in vivo and in vitro), predominately because of the presence of transition-metal catalysts, and have been shown to cause some cytotoxicity at elevated concentrations (16).

The use of biological materials such as proteins from egg shells has also been reported as a reinforcing agent for PCL-based nanofibers (17). Although the mechanical and interfacial properties of the composites were improved, the incorporation of such soluble polymers in the PCL matrixes required special manufacturing protocols.

The incorporation of cellulose nanocrystals (CNXs) into polymer nanofibers would be advantageous over CNTs because the precursor cellulose in CNXs is obtained from an abundant bioresource. Also, CNXs are less expensive, simple to produce, and, most importantly, biocompatible and biodegradable. Excellent chemical and thermomechanical properties of CNXs have been reported (18, 19), making them suitable candidates as a reinforcing, disperse phase in

* Corresponding author. E-mail: ojrojas@ncsu.edu.
Received for review May 30, 2009 and accepted August 15, 2009
[†] North Carolina State University.
[‡] Helsinki University of Technology.
DOI: 10.1021/am9003705

Published on Web 08/28/2009

Table 1. Properties of the PCL Solution in 4:1 DCM/DMF (15% w/w) and Respective Dispersions with Different CNX Loadings (Determined at 25 °C)

sample	CNX content (%)	viscosity (Pa · s)	conductivity (μS/cm)	surface tension (mN/m)
neat PCL		0.59	0.31	32.5
PCL with unmodified CNX	2.5	2.41	0.97	33.6
	5.0	1.21	4.96	33.1
	7.5	0.96	0.22	32.5
PCL with PCL-grafted CNX	2.5	0.42	2.82	32.2
	5.0	0.62	3.07	32.9
	7.5	n/a	n/a	n/a

polymer matrixes (20−23). CNXs can be produced from a variety of cellulose sources including wood, cotton, sisal, ramie, tunicate, fungi, or bacteria (24). Bacterial CNXs have been successfully incorporated into hydrophilic poly(ethylene oxide) nanofibers, and increases in the modulus, strength, and strain at break were observed (17). Recently, we have successfully used CNXs as a reinforcing phase in composites made from synthetic hydrophobic matrixes (25).

In this work, we propose a novel combination of biodegradable CNXs from natural fibers as reinforcing materials in PCL nanofibers via electrospinning. The resulting composites were developed to overcome the otherwise low mechanical strength of neat PCL nonwoven webs. The grafting of low-molecular-weight PCL diol chains onto the surfaces of CNXs and their incorporation in electrospun PCL matrixes were also investigated. The effect of such a functionalization was addressed in an effort to improve their compatibility with the continuous phase. Finally, the main structural and thermomechanical features of the developed composite nanofibers were addressed for various CNX loadings.

EXPERIMENTAL SECTION

Materials and Methods. ***Materials.*** Pure ramie fibers were obtained from Stucken Melchers GmbH & Co. (Germany). Toluene 2,4-diisocyanate (2,4-TDI; 95%), polycaprolactone (PCL; 80 000 g/mol), PCL diol (2000 g/mol), toluene (anhydrous, 99.8%), and dichloromethane (DCM; 99.5%), were all obtained from Sigma-Aldrich. Sulfuric acid (95%), acetic acid (glacial), triethylamine (TEA; 99.5%), acetone (99%), *N*,*N*-dimethylformamide (DMF; 99%), sodium hydroxide pellets, and sodium chlorite were all purchased from Fischer Scientific. All solvents were dried over molecular sieves (3 Å, 4−8 mesh beads, Sigma-Aldrich) for 48 h before use.

CNXs. The procedure for preparing ramie CNXs was adapted from Habibi et al. (26). In short, ramie fibers were first treated for 2 h with a 4 wt % NaOH solution at 80 °C to purify cellulose fibers from residual additives. The purified ramie fibers obtained after repeating the previous procedure were then acid-hydrolyzed with 65 wt % sulfuric acid (55 °C, 45 min). The resulting dispersion was filtered into ∼500 g of ice cubes and washed with distilled water until neutral pH by successive centrifugation at 12 000 rpm at 10 °C for 20 min. Finally, dialysis for 1 week against deionized water with a 3500 MWCO dialysis membrane was performed to remove trace amounts of residual sulfuric acid.

Surface Grafting. CNXs from the above procedure were grafted with PCL diols and also used to manufacture the composite nanofibers. Grafting PCL onto CNXs was performed according to a slightly modified procedure reported by Habibi et al. (23) using TDI as the coupling agent. A total of 2 g of ramie CNXs was solvent-exchanged from water to acetone (three times), then to toluene, and to anhydrous toluene by using successive centrifugations (12 000 rpm at 10 °C for 20 min). The resulting CNXs were placed in 100 mL of anhydrous toluene in a 250 mL flask equipped with a reflux condenser under argon gas and heated to 75 °C with vigorous stirring. A total of 2 mL of TEA was added followed by the dropwise incorporation of 12.3 mmol of 2,4-TDI. The mixture was left to react for 24 h at 75 °C and then centrifuged three times with anhydrous toluene and once with acetone to remove unreacted 2,4-TDI. A total of 24.6 g of PCL diol and 2 mL of TEA were dissolved in 100 mL of anhydrous toluene in a 250 mL flask equipped with a reflux condenser under an argon atmosphere and heated to 75 °C; then, 2,4-TDI-modified CNXs, prepared previously, were added, and the reaction was left to proceed for 5 days with stirring. The reaction mixture was then centrifuged with toluene (three times) and dried overnight under vacuum at 40 °C. The resulting PCL-modified CNXs were Soxhlet-extracted with DCM to remove ungrafted PCL diol and dried in a vacuum oven overnight at 40 °C. The grafted CNXs were hydrophobic and dispersible in DCM.

Preparation and Characterization of the Dispersions. **1. Dispersion of Unmodified CNXs in PCL.** Aqueous dispersions of unmodified CNXs were solvent-exchanged from water to DMF by rotary evaporation. First, aqueous dispersions were concentrated in a rotary evaporator, then a volume of DMF was added, and the remaining water was subsequently evaporated to a desired final volume of DMF. Desired amounts of unmodified CNXs in DMF were sonicated for a few minutes using an OMNI-Ruptor 250 Ultrasonic Homogenizer before adding them to PCL solutions. A total of 15 g of PCL was dissolved in DCM, and then freshly sonicated CNX dispersions were mixed to produce dispersions that lead to CNXs loadings of 2.5, 5.0, and 7.5% in PCL. These dispersions (up to CNX content of 7.5%) were found to be colloidally stable over long periods of time. **2. Dispersion of Grafted CNXs in PCL.** Hydrophobic, PCL-grafted CNXs were also dispersed directly in DMF. Desired amounts of PCL-grafted CNXs in DMF were sonicated as previously described before adding them to PCL solutions. A total of 15 g of PCL was dissolved in DCM, and then freshly sonicated CNX dispersions were mixed to produce dispersions that lead to CNX loadings of 2.5 and 5.0% in PCL. In this case, the dispersions were only colloidally stable over long periods of time up to CNX contents of 5.0%. **3. Characterization of the CNX Dispersions.** The viscosity, conductivity, and surface tension of the final dispersions were determined at 25 °C by a programmable rheometer (AR2000, TA Instruments), a conductivity meter (Corning Inc., model 441), and a Du Noüy ring (Fisher tensiomat, model 21), respectively (see Table 1).

Electrospinning. Nonwoven nanofiber webs of neat PCL and PCL reinforced with (unmodified and PCL-grafted) ramie CNXs were produced via electrospinning (27). The strength of the electric field used during electrospinning was varied from

0.5 to 1.0 kV/cm between a positive electrode attached to the tip of a syringe needle connected to a pump and a grounded collector plate. Ramie CNXs were dispersed in a 15% (w/w) PCL solution (4:1 DCM/DMF solvent) at loads corresponding to 2.5, 5.0, and 7.5% (based on the total mixture weight). Freshly prepared dispersions were electrospun with varying flow rates (0.8−1.0 mL/h) and tip-to-collector separations (10−20 cm). The produced nanofiber webs were collected during processing times that were varied between 30 min and 4 h, depending on the desired web film thickness.

Transmission Electron Microscopy (TEM). Drops of aqueous dispersions of unmodified CNXs (0.01% w/v) were deposited on carbon-coated electron microscope grids (Protochips Inc.), negatively stained with uranyl acetate, and allowed to dry. The grids were observed with a Hitachi HF-2000 transmission electron microscope operated at an accelerating voltage of 80 kV.

Scanning Electron Microscopy (SEM). A Hitachi S-3200N variable-pressure scanning electron microscope was used to image the nanofiber webs formed after electrospinning. The nanofibers, which were collected on aluminum foil placed on the collector, were shadowed with a layer (∼150 Å thick) of gold−palladium and observed under a microscope working distance between 3 and 60 mm using an accelerating voltage from 0.3 to 30 kV. The nanofiber diameter distribution was estimated using UTHSCSA Image Tool for Windows freeware and by manually measuring individual diameters across the image. Size distribution measurements were conducted for each sample considering ca. 40 nanofibers from 10 000× images (shown in Figure 5).

Differential Scanning Calorimetry (DSC) and Thermogravimetric Analysis (TGA). DSC was performed using a TA Instruments Q100 differential scanning calorimeter. In a typical experiment, ca. 10 mg of sample was placed in the DSC cell and heated from −100 to +100 °C (heating rate of 10 °C/min). The melting temperature T_m was taken as the onset temperature of the melting endotherm. For crystallization studies, the sample was first heated to 100 °C, kept at this temperature for 5 min to ensure complete melting of PCL, and then cooled to 0 °C at a cooling rate of 10 °C/min. The crystallization temperature T_c was taken as the peak of the crystallization exotherm. TGA was performed using a TA Instruments Q500 thermogravimetric analyzer. Data were collected after placing ca. 10 mg of sample in a clean platinum pan and heating from ambient temperature to 600 °C (heating rate of 20 °C/min).

Dynamic Mechanical Analysis (DMA). DMA was performed in tensile mode (TA Instruments Q800). The measurements were carried out at a constant frequency of 1 Hz and a strain amplitude of 0.03%, for a temperature range of −100 to +100 °C, using a heating rate of 3 °C/min and a gap between jaws of 10 mm. Nonlinear deformations (tensile tests) were obtained in controlled force mode at a temperature of 25 °C and ramping at 3 N/min. The DMA samples consisted of 6-mm strips cut from the respective nanofiber webs. Three samples were used to characterize each material.

RESULTS AND DISCUSSION

Characterization of CNXs. CNXs were produced by sulfuric acid hydrolysis from ramie fibers. The morphology of these rodlike nanocrystals was characterized by TEM, as shown in Figure 1. The CNX dimensions, which were typically 3−10 nm in diameter and 100−250 nm in length, agreed well with the literature values reported for ramie CNXs produced under the same conditions (23, 26).

One of the challenges in preparing composites with hydrophilic CNXs in hydrophobic polymer matrixes is the low interfacial compatibility that may lead to poor composite mechanical strength. To overcome this issue, surface chemical modification of CNXs with polymer grafts of the same chemical nature as that of the matrix was carried out. Polymer grafting can be accomplished by either "grafting-onto" (28) or "grafting from" (29) approaches. In this work, we evaluated the effect of grafting low-molecular-weight PCL diol onto ramie CNXs. Surface modification was carried out following the "grafting-onto" method using 2,4-TDI as a coupling agent. The first step required the reaction of the surface hydroxyl groups of CNXs with one isocyanate functionality of 2,4-TDI (to produce TDI-*g*-CNXs). During the second step, the unreacted second isocyanate of 2,4-TDI was then reacted with the end hydroxyl groups of PCL diol to graft the PCL chain onto the nanocrystals. The isocyanate functionality at the 4 position is reported to react first as this position is 7 times more reactive than the one at 2 position (30).

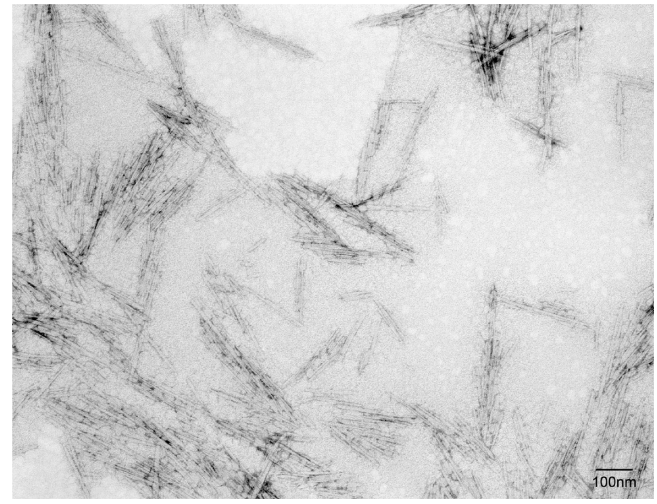

FIGURE 1. TEM image of ramie CNXs.

The accomplished surface grafting was confirmed by FTIR (see Figure 2). First, the grafting of the coupling agent TDI at the surface of CNXs was confirmed by the presence of new peaks corresponding to the carbonyl stretch, amide stretch, and amine bend for grafted 2,4-TDI (at wavenumbers of 1710, 1596, and 1537 cm^{-1}, respectively), in comparison with the spectrum of unmodified ramie CNXs. The peak at 2270 cm^{-1} was attributed to the unreacted isocyanate functionality. After the reaction of TDI-*g*-CNXs with PCL diol, the same distinctive peaks were seen as those for the grafted TDI; however, a new and intense peak at 1720 cm^{-1} was observed and ascribed to the ester carbonyls in PCL chains. It was also noted that there was a significant decrease in the intensity of the isocyanate stretch at 2270 cm^{-1}, confirming attachment of PCL diol.

Successful PCL grafting onto CNXs was also verified by TGA, as shown in the thermograms of freeze-dried unmodified and PCL-grafted CNXs (see Figure 3). The thermogram of unmodified CNX showed the typical degradation profile of CNXs with sulfate groups introduced during fiber hydrolysis with sulfuric acid (see Figure 3A) (31). The differential thermogram with a peak around 300 °C (see Figure 3B)

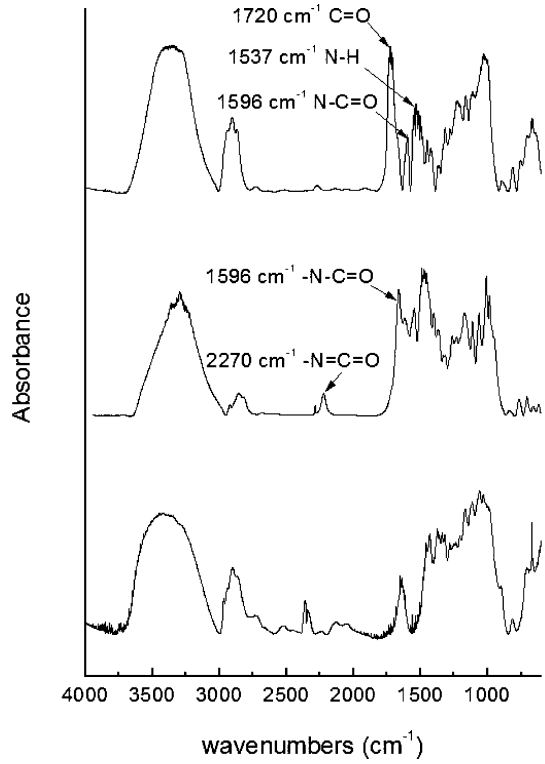

FIGURE 2. FTIR spectra of unmodified CNX (lower), CNX after reaction with TDI (or before grafting) (middle), and PCL-grafted CNXs (upper).

corresponded to cellulose degradation, which typically occurs between 250 and 325 °C because of its depolymerization, dehydration, and decomposition of glycosyl units followed by the formation of a charred residue. The small shoulder above 325 °C was ascribed to the oxidation and breakdown of the charred residue to lower molecular weight gaseous products. Compared to unmodified CNXs, the thermogram of PCL-grafted CNXs showed distinct degradation behavior (see Figure 3A). The peak around 375 °C observed in Figure 3B was attributed to the degradation of grafted PCL chains, which corresponded to the thermogram peak of neat PCL diol that was used as a reference (Figure 3B). Two additional peaks at 275 and 325 °C were observed in the thermogram of PCL-grafted CNXs. These peaks were related to the effect of unreacted isocyanate linked to CNXs (see Figure 2) and grafted PCL diol onto the CNXs, respectively.

From the weight loss recorded with TGA for PCL-grafted CNXs, the grafting yield was estimated to be 30%, which is in agreement with the weight gain determined after CNX grafting by analytical gravimetry. From this value and with the amount of available hydroxyl groups (carbon 6 of glucopyranose) on the surface of CNXs, the grafting density was calculated to be ca. 4.5%. This low grafting density is typical of "grafting onto" methods, which are limited because of high steric hindrance and entropy considerations (28).

Production and Characterization of Composite Nanofibers. Nonwoven nanofiber webs of neat PCL and PCL reinforced with 2.5, 5.0, and 7.5% (w/w) unmodified and PCL-grafted ramie CNXs were produced via electrospinning. The operating conditions for the production of these nanofibers were thoroughly investigated. The optimum voltage range was found to be between 10 and 15 kV at a distance between the syringe tip and the collector of 15−20 cm (corresponding to an electric field strength of 0.65−0.75 kV/cm). The nanofibers were collected on an aluminum foil, and the morphologies of the nanofiber webs were characterized by SEM. Figure 4 shows typical images of the collected PCL nanofiber webs with and without CNX reinforcement. The corresponding fiber diameter histograms are given in Figure 5.

Figure 4A shows a typical SEM image of neat PCL nanofibers produced under the stated conditions. The fibers were homogeneous, and their diameters were in the nanoscale range. Some anomalies such as beads and/or diameter engrossment within single fibers were observed, which are typical of these systems (27). By variation of the electric field strength from 0.65 to 0.75 kV/cm, a slight shift in distribution toward smaller fiber diameters was observed (see Figure 5A,B, respectively). A reduction in the average fiber diameter from 210 nm (0.65 kV/cm) to 180 nm (0.75 kV/cm) was observed. This reduction in the fiber diameter can be explained by the electrically induced stretching of fibers during the electrospinning process, as reported in other systems (32).

Parts B−D of Figure 4 show PCL nanofibers reinforced with 2.5, 5.0, and 7.5% (w/w), never-dried, unmodified CNXs. The corresponding diameter frequency distribution is reported in Figure 5C−E. All CNX-loaded PCL fibers were nanometric in size, and their surfaces appeared to be smooth, except those filled with 7.5% CNXs. By the addition of 2.5% of CNXs, thinner fibers were produced, as compared to unfilled PCL nanofibers. In fact, the diameter of the nanofibers produced under the same conditions decreased from 210 to 120 nm for neat and 2.5% PCL-reinforced fibers, respectively. This observed reduction in the diameter with the (low-level) addition of reinforcing CNXs can be attributed to the effect of the increased viscosity of the latter dispersion during electrospinning, as reported in Table 1. Although the viscosities of all dispersions were greater than that of neat PCL solutions, a decrease in the viscosity was observed relative to unmodified CNX loadings. This effect may be attributed to the formation of CNX aggregates in the case of high loads, which were not apparent by visual inspection. In addition, the ionic strength of the electrospinning solution brought about by the negatively charged CNXs, from the sulfate groups grafted during the hydrolysis process, could also contribute with the reduction in the diameter of the electrospun nanofibers (33). This is because the increase in the electrostatic charge density of the electrospinning solution induces more extensive filament stretching during jet whipping. However, as the CNX concentration increased, the effect of the charge density on the produced nanofiber diameter was offset by a lower dispersion viscosity (see Figure 5D,E, where larger fiber diameters are observed). According to the aspect ratio of the used CNXs, the percolation threshold was calculated to be around 3% (34). Above

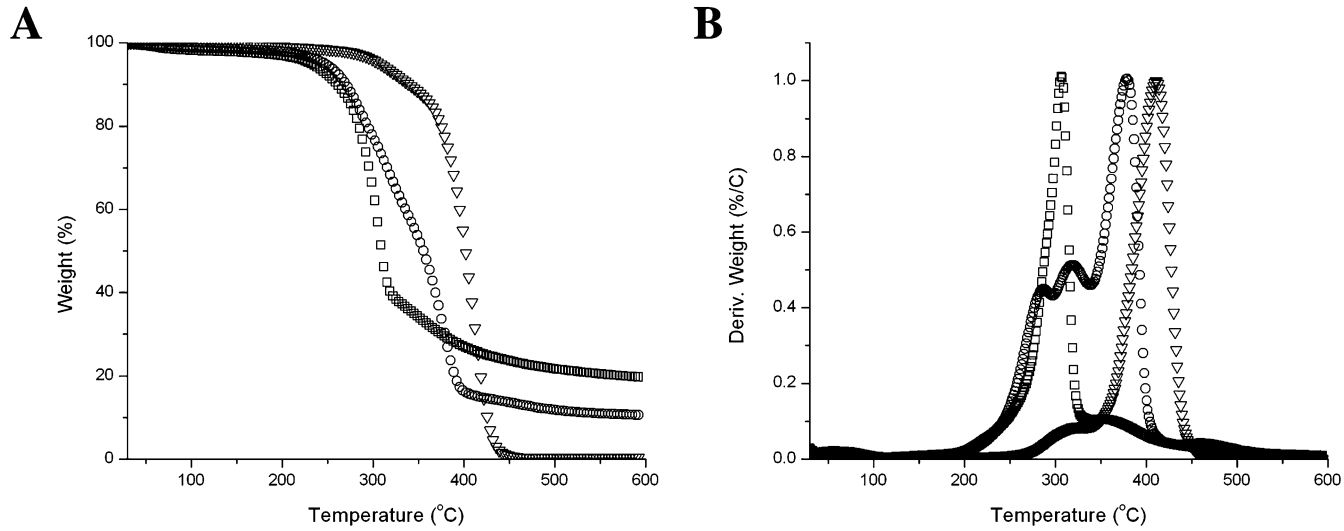

FIGURE 3. TGA (A) and differential thermogravimetry (B) curves of PCl diol (▽), unmodified CNX (□), and PCL-grafted CNX (○).

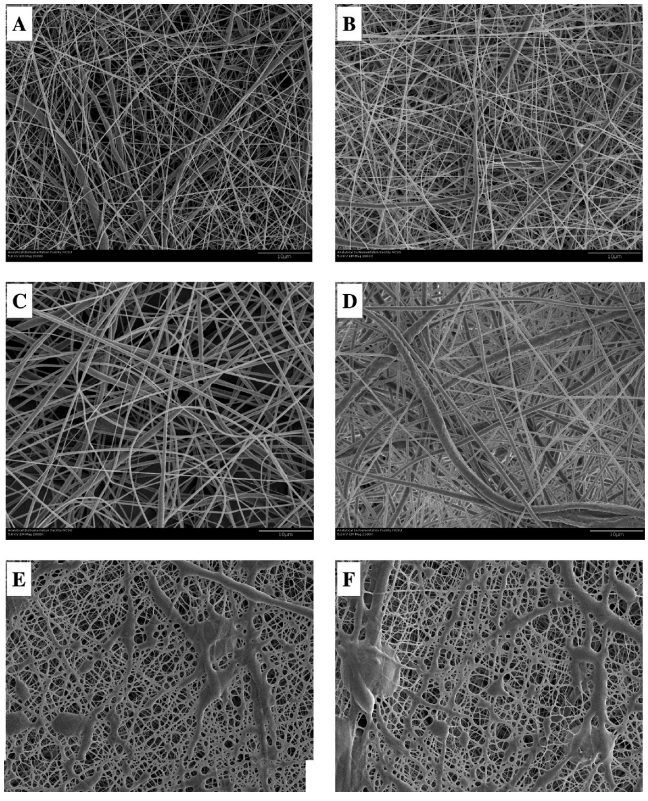

FIGURE 4. SEM images of nanofiber webs produced by electrospinning at an electrical field strength of 0.65 kV/cm and a flow rate 1.0 mL/h. Shown are neat PCL nanofibers (A) and PCL nanofibers reinforced with unmodified CNXs at weight loads of 2.5 (B), 5.0 (C), and 7.5% (D). PCL nanofibers reinforced with grafted-CNXs at 2.5 (E) and 5% (F) are also included.

this concentration, the likelihood of CNX aggregation is expected to increase, and therefore the fiber diameter may increase. Accordingly, the contribution of CNX overlapping adds to the effect described earlier to produce larger fiber diameters (see Figure 5C,E).

Parts E and F of Figure 4 show SEM images of electrospun nanofiber webs of PCL reinforced with 2.5 and 5.0% PCL-grafted (ramie) CNXs produced at electrospinning conditions corresponding to those found as optimum in the case of neat PCL. While the general aspect and morphologies of the unmodified CNX-loaded PCL nanofibers were preserved compared to neat PCL nanofibers, the addition of PCL-grafted CNXs to the PCL matrix produced different morphological features. Despite the fact that a precursor random nanofibrillar structure seemed to take place (see Figure 4E,F), the nanofibers were annealed and formed a more continuous film with many broad nodes. Therefore, the diameter size distribution of nanofibers could not be evaluated and compared to other nonwoven PCL webs. This phenomenon can be explained by three main reasons. First, suspension instabilities caused aggregation by the reduction in the polarity of the dispersion. Second, the electrospinning conditions were optimized for the high-molecular-weight PCL matrix (which also were suitable for processing PCL with unmodified CNXs). In the case of CNX grafted with short PCL chains, the required conditions to preserve the nanofiber integrity are expected to be different because of the different respective rheological behavior. Finally, the different morphologies observed for composite fibers with grafted CNX can be a consequence of the different crystallization rates for different PCL chains (those of the PCL matrix and the grafted chains on CNXs). Such features in the crystallization rate are expected to occur because of the different molecular masses (80 000 for the PCL matrix and 2000 for the PCL grafts). As a consequence, the solution jet from the high-molecular-weight PCL matrix was elongated and solidified rapidly after spinning from the syringe tip, while the grafted chains on CNXs may have taken more time to crystallize and probably did not elongate during the electrospinning process.

Thermomechanical Properties of PCL-Based Fiber Nanocomposites. In order to determine the reinforcing effect of CNXs and PCL-grafted CNXs on the thermal and mechanical properties of PCL nanofibers, DSC and DMA tests were conducted. Table 2 shows the melting temperature (T_m), degree of crystallinity (χ_c), and crystallization temperature (T_c) for all composite fibers studied. An increase in the degree of crystallinity (χ_c) was observed when comparing bulk, as-received PCL and electrospun webs from

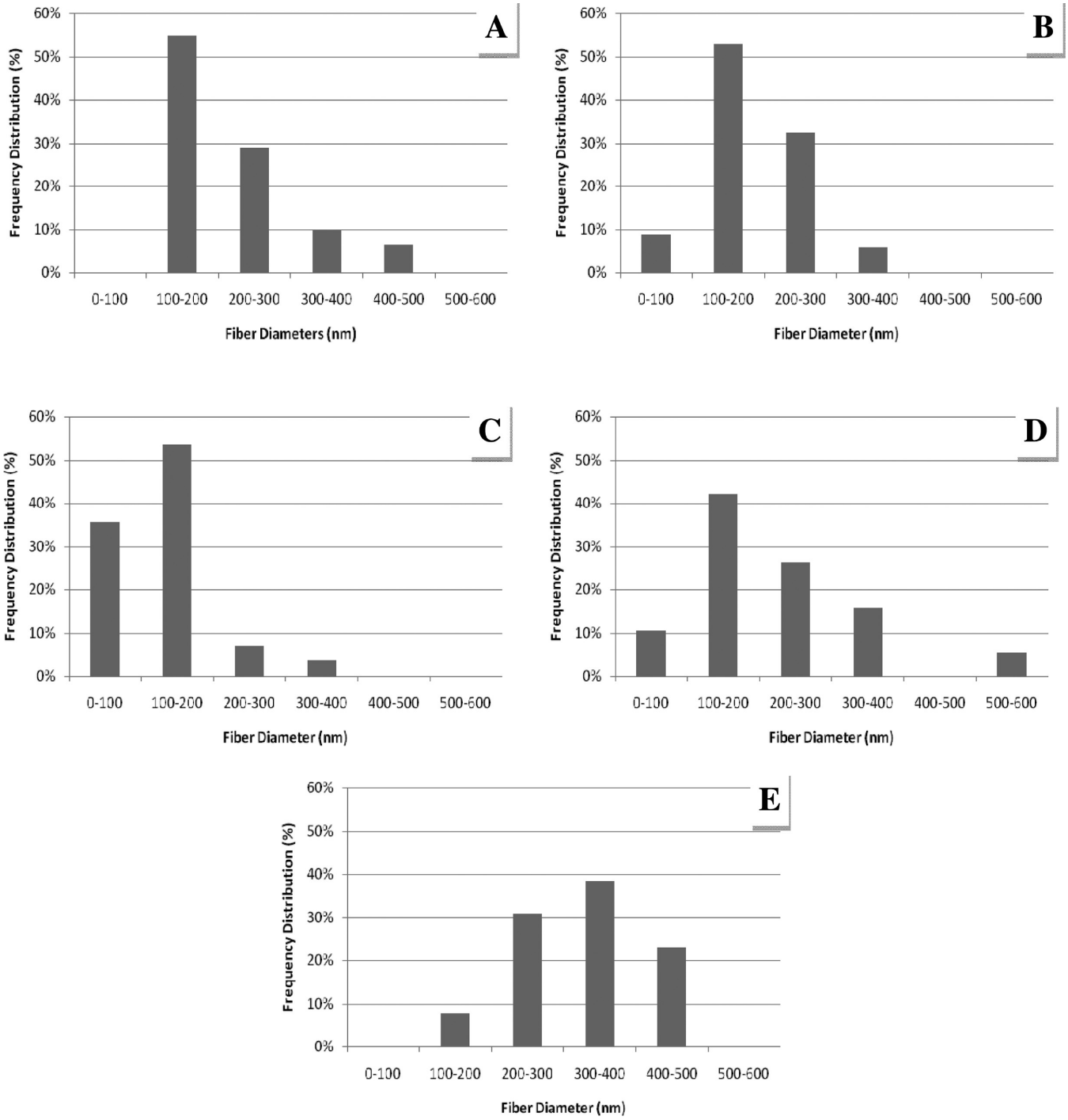

FIGURE 5. Diameter frequency distribution of nanofibers of neat PCL obtained at a electrospinning flow rate of 0.8 mL/h and electrical field strengths of 0.65 (A) and 0.75 (B) kV/cm. The histograms corresponding to PCL reinforced with 2.5% (C), 5.0% (D), and 7.5% (E) ramie CNXs (at 0.65 kV/cm and 0.8 mL/h) are also included.

the same polymer (0.51 and 0.55, respectively). The corresponding melting temperatures (T_m) slightly decreased (from 53.4 to 52.2 °C), as expected. On the basis of these results, it is hypothesized that the electrospinning process restrained the mobility of the polymer chains in such a way that more but smaller PCL crystallites were formed within the electrospun nanofibers.

The addition of CNXs into PCL produced minimal changes in the thermal properties of the electrospun fibers. Only small differences in the melting temperature (T_m) as well as the degree of crystalinity were observed when unmodified CNXs were used as reinforcements. A larger T_m and degree of crystallinity were expected because in the case of composite cast films CNXs acted as nucleating agents in the crystallization of PCL (35, 36). In associated, very slow processes, the lattice structure and the differences in the chemical composition of CNXs and PCL were beneficial for the matrix to nucleate on the surface of CNXs. It was observed that in cast films the matrix crystals nucleated epitaxially on the surface of the added CNXs and crystal

Table 2. Summary of DSC Results for Commercial PCL and PCL Nanofiber Webs after Electrospinning (ES) with and without Reinforcing Ramie CNXs (Unmodified and PCL-Grafted)

sample	CNX content (%)	T_m	ΔH	X_c[a]	T_c
commercial PCL		53.40	80.30	0.51	26.02
ES-PCL		52.20	86.00	0.55	28.07
ES-PCL with unmodified CNX	2.5	53.23	79.81	0.52	38.85
	5.0	53.71	79.56	0.53	37.34
	7.5	53.13	77.97	0.54	35.47
ES-PCL with PCL-grafted CNX	2.5	52.20	70.19	0.46	32.79
	5.0	51.80	70.53	0.47	33.32
	7.5	n/a	n/a	n/a	n/a

[a] $X_c = \Delta H/[\Delta H_{100\%}*(1 - w)]$, where $\Delta H_{100\%\ PCL} = 157$ J/g (35).

growth occurred radially, relative to the axis of CNXs. Therefore, a transcrystalline layer was formed. In contrast, during electrospinning, the very high shear stress and the very fast solvent evaporation induced rapid crystallization before the polymer nanofibers reached the collector. This fast process, as well as the volume restriction within the nanofibers, was a possible cause for restricted crystallite growth.

In contrast to the case of unmodified CNXs, a reduction in the degree of crystallinity and melting temperature of PCL reinforced with PCL-grafted CNXs was observed. This fact can be attributed to the effect of grafted, low-molecular-mass chains on CNXs that impairs the formation of PCL crystallites during electrospinning. This is consistent with observations made for cast films with similar composition; it was observed that grafting interrupted the nucleation effect of CNXs. Also, it can be argued that during the electrospinning the crystallization of the grafted short chains was delayed. This last phenomenon was confirmed by the observed crystallization temperature of the nanofiber webs: significant differences in crystallization temperatures were evident, as seen in Table 2 and in agreement with the results reported in the case of cast films (35, 36). Similar T_c values measured for cast films and electrospun webs are noteworthy because in the latter case the nanofiber webs melted and crystallized more like a cast film. In contrast, and as a confirmation of the previous hypothesis, an important increase in T_c was observed for electrospun PCL filled with unmodified CNXs. In fact, the T_c's of nanofiber webs shifted significantly (by 11 °C), after loading PCL with unmodified CNXs.

The mechanical properties of nanofibers have important roles in many applications, including mechanical support in cell growth and migration in scaffolds. However, the mechanical properties of neat PCL electrospun fiber webs are known to be deficient. Several studies have explored various blends and/or reinforcing systems, and various processing parameters and postprocessing treatments have been proposed to improve associated mechanical properties (8, 9, 11, 17). Electrospun fibers form nanostructured networks that are expected to influence mechanical properties such as the tensile strength, elongation, etc. Elastomer-based electrospun fibers have shown a 40% reduction in the peak tensile strength and 60% reduction in elongation at maximum applied stress compared to cast films. According to Wang et al., the mechanical properties of electrospun nanofiber webs are closely related to the fiber orientation, bonding between fibers, and fiber slippage rather than the mechanical properties of individual fibers within the web (37).

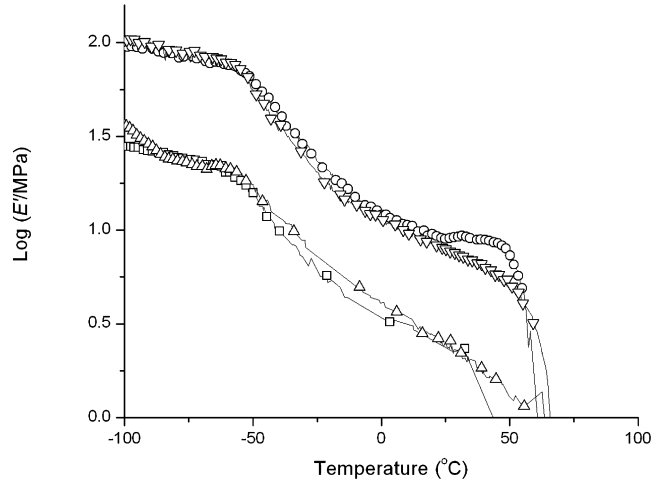

FIGURE 6. Change in the storage modulus with temperature for nanofiber webs of neat PCL (□) and PCL loaded with 2.5% (○), 5% (Δ), and 7.5% (▽) of unmodified ramie CNXs.

In order to evaluate the mechanical properties of nanofiber webs from PCL and CNX-filled PCL, longer electrospinning collection times were used to produce suitable, thicker samples. In these measurements, nanofiber samples were limited to those from neat PCL and PCL filled with unmodified CNXs (so as to avoid complicating effects from the different morphological features observed in nanocomposites with PCL-grafted CNXs). The morphologies of such thicker (0.15 mm) webs were observed under SEM, and the preservation of the nanofibrillar structure was confirmed. DMA measurements were performed on these nanofiber webs, and the change of the storage modulus with temperature is reported in Figure 6. The storage modulus curves displayed the typical behavior of semicrystalline polymers with four distinctive zones. At low temperature (below −60 °C), the modulus slightly decreased with temperature. This observed limited temperature effect is explained by the fact that the polymer was in the glassy state and molecular motions were largely restricted to vibration and short-range rotation. Around −60 °C, a transition showed as a sharp drop in the storage modulus was observed. At this temperature, the main relaxation process corresponded to amorphous PCL domains associated with the glass transition of the polymer. At higher temperatures range, −60 to 40 °C, the storage tensile modulus decreased due to the progressive melting of the PCL matrix. Here amorphous, rubbery, and crystalline domains coexisted. At higher temperatures (above 50−60 °C), the modulus dropped sharply and unrecoverable deformations occurred because of the complete melting of the crystalline zones of the PCL matrix.

A significant increase in the storage modulus was observed in the case of webs of PCL filled with unmodified CNXs (2.5 and 7.5%) in comparison with neat PCL. In the

Table 3. Results from Tensile Tests of Electrospun PCL Nanofiber Webs without Reinforcing CNX (ES-PCL) and with Reinforcing (Unmodified) CNXs (ES-PCL−CNX) Added at Various Concentrations

sample	CNX content (%)	Young's modulus (MPa)	strength (MPa)	strain at break (%)
ES-PCL		3.89 ± 0.10	1.10 ± 0.08	43.5 ± 10.4
ES-PCL−CNX	2.5	6.54 ± 0.26	1.51 ± 0.06	64.8 ± 2.4
	5.0	3.94 ± 0.58	0.86 ± 0.08	82.6 ± 8.2
	7.5	6.26 ± 0.73	1.32 ± 0.21	85.8 ± 14.4

case of PCL webs with 2.5% unmodified CNXs, the reinforcing effect resulted from the filler loading, but it also can be partially attributed to the smaller fiber diameters observed at this load during electrospinning (relative to other CNX loads tested). As noted earlier, the fiber diameters tended to increase with the reinforcement load. Smaller fiber diameters yielded higher overall relative bonded areas between fibers because of the increased surface area, bonding density, and better distribution of bonds. In the case of 5% CNX load in PCL, variations in the storage modulus compared well with the corresponding profile obtained for the neat PCL matrix. According to the morphology results presented previously, at this loading the fiber diameter was similar to that of neat electrospun PCL. At 7.5% CNX loading, the storage modulus increased compared to that of neat PCL. This was despite the fact that the nanofiber diameter was larger at this CNX load. Therefore, the improved mechanical behavior in this case can be related to the reinforcing contribution of CNXs within the fiber (intrinsic strength). From these results, it becomes clear that the effects of CNXs and the fiber diameter on the mechanical properties of the nanocomposites are intimately related. It is expected that different optimum CNX loadings apply to different fiber diameters.

PCL nanofiber webs reinforced with PCL-grafted CNXs presented poor mechanical properties (results not presented). In this case, the storage modulus dropped drastically above the glassy transition and did not follow the trend observed in other PCL-based nanofiber webs. The poor mechanical properties after loading of modified CNXs are related to the heterogeneous morphologies of the webs, which contain both nanofibrillar and annealed structures. The defective morphology in this case makes the adhesion within the web and stress transfer deficient.

The behavior of electrospun webs under nonlinear deformations was also investigated. Table 3 summarizes the results (Young's modulus, strength, and strain at rupture) obtained from these tensile tests. The neat PCL nanofiber webs showed an ultimate strength of 1.10 MPa and a maximum strain of 43.5%. Young's modulus was calculated to be 3.89 MPa. With the incorporation of unmodified CNXs, a distinctive increase of these mechanical properties was realized (for loadings of 2.5 and 7.5%). The system with 5% CNX loading gave mechanical properties similar to those of the neat PCL webs. Nanofiber webs reinforced with 2.5% unmodified CNXs showed the most notable increase (ca. 1.5-fold increase in Young's modulus and the ultimate strength compared to those of the neat PCL webs). If it is assumed that the slippage between fibers and fiber bonding were uniform over all nanofiber webs, it is clear that the mechanical properties of the PCL−CNX composites (nanofiber webs) were effectively improved by incorporating unmodified CNXs.

CONCLUSIONS

Nanofiber web composites based on biodegradable PCL and CNXs were successfully produced via the electrospinning technique. Chemical grafting of CNXs with short PCL chains was used in an attempt to obtain better compatibility between the hydrophobic PCL matrix and the hydrophilic CNX disperse phases. It was demonstrated that CNXs can be used effectively as reinforcing material in electrospun PCL and to produce nanofibers with unique structural properties. Homogeneous nanofibers with diameters in the nanoscale and improved thermomechanical properties were obtained when unmodified CNXs were incorporated in the PCL matrix. When short PCL chains were grafted onto the surface of CNXs, annealed fibrillar morphologies were obtained. The interfering effect of short PCL chains during the electrospinning process was elucidated. The differences in the crystallization rates of the high- and low-molecular-mass PCL in the matrix and in the CNX grafts impaired the properties of PCL filled with PCL-grafted CNXs.

Finally, a significant increase in the storage modulus at all temperatures tested and nonlinear deformation strength properties were observed when CNXs were incorporated in the PCL nanofibers. The reinforcement effect of CNXs was demonstrated and explained in terms of differences in the fiber diameter, CNX loading, and crystallization processes.

Acknowledgment. The authors are thankful to the National Research Initiative of the USDA Cooperative State Research, Education and Extension Service (Grant 2007-35504-18290), and the USDA NNF program (Grant 2007-38420-17772) for their financial support.

REFERENCES AND NOTES

(1) Boland, E. D.; Pawlowski, K. J.; Barnes, C. P.; Simpson, D. G.; Wnek, G. E.; Bowlin, G. L. In *Polymeric Nanofibers*; ACS Symposium Series 918; Reneker, D. H., Fong, H., Eds.; American Chemical Society: Washington, DC, 2006; pp 188−204.
(2) Buschle-Diller, G. ; Hawkins, A.; Cooper, J. In *Modified Fibers with Medical and Specialty Applications*; Edwards, V., Buschle-Diller, G., Goheen, S. C., Eds.; Springer: Dordrecht, The Netherlands, 2006; pp 67−80.
(3) Chen, M.; Patra, P. K.; Warner, S. B.; Bhowmick, S. *Biophys. Rev. Lett.* **2006**, *1*, 189–214.
(4) Gu, S. *Gaofenzi Tongbao* **2005**, *28*, 13–17.
(5) Agarwal, S.; Wendorff, J. H.; Greiner, A. *Polymer* **2008**, *49*, 5603–5621.
(6) Kumbar, S. G.; James, R.; Nukavarapu, S. P.; Laurencin, C. T. *Biomed. Mater.* **2008**, *3*, 034002/1–034002/15.
(7) Venugopal, J.; Vadgama, P.; Kumar, T. S. S.; Ramakrishna, S. *Nanotechnology* **2007**, *18*, 055101/1–055101/8.
(8) Bajgai, M. P.; Aryal, S.; Bhattarai, S. R.; Bahadur, K. C. R.; Kim, K.-W.; Kim, H. Y. *J. Appl. Polym. Sci.* **2008**, *108*, 1447–1454.
(9) Bosworth, L.; Clegg, P.; Downes, S. *Int. J. Nano Biomater.* **2007**, *1*, 263–279.
(10) Srouji, S.; Kizhner, T.; Suss-Tobi, E.; Livne, E.; Zussman, E. *J. Mater. Sci.: Mater. Med.* **2008**, *19*, 1249–1255.
(11) Ghasemi-Mobarakeh, L.; Prabhakaran, M. P.; Morshed, M.; Nasr-

Esfahani, M.-H.; Ramakrishna, S. *Biomaterials* **2008**, *29*, 4532–4539.
(12) Venugopal, J. R.; Low, S.; Choon, A. T.; Kumar, A. B.; Ramakrishna, S. *Artificial Organs* **2008**, *32*, 388–397.
(13) Saeed, K.; Park, S.-Y.; Lee, H.-J.; Baek, J.-B.; Huh, W.-S. *Polymer* **2006**, *47*, 8019–8025.
(14) Dean, D.; Jose, M. V.; Abdalla, M. A.; Green, K.; Bellis, S.; Thomas, V.; Vohra, Y.; Nyairo, E. *PMSE Prepr.* **2005**, *93*, 507–508.
(15) Barron, A. R.; Khan, M. R. *Adv. Mater. Processes* **2008**, *166*, 41–43.
(16) Smart, S. K.; Cassady, A. I.; Lu, G. Q.; Martin, D. J. *Carbon* **2006**, *44*, 1034–1047.
(17) GeunHyung, K.; Taijin, M.; Su, A. P.; Wan, D. K.; Young, H. K. *Biomed. Mater.* **2007**, *2*, 250–256.
(18) Kamel, S. *eXPRESS Polym. Lett.* **2007**, *1*, 546–575.
(19) Samir, M. A. S. A.; Alloin, F.; Dufresne, A. *Biomacromolecules* **2005**, *6*, 612–626.
(20) Bondeson, D.; Oksman, K. *Compos. Interfaces* **2007**, *14*, 617–630.
(21) Dufresne, A. *Can. J. Chem.* **2008**, *86*, 484–494.
(22) Mathew, A. P.; Thielemans, W.; Dufresne, A. *J. Appl. Polym. Sci.* **2008**, *109*, 4065–4074.
(23) Roohani, M.; Habibi, Y.; Belgacem, N. M.; Ebrahim, G.; Karimi, A. N.; Dufresne, A. *Eur. Polym. J.* **2008**, *44*, 2489–2498.
(24) O'Sullivan, A. C. *Cellulose* **1997**, *4*, 173–207.
(25) Rojas, J. O.; Montero, A. G.; Habibi, Y. *J. Appl. Polym. Sci.* **2009**, *113*, 927–935.
(26) Habibi, Y.; Foulon, L.; Aguie-Beghin, V.; Molinari, M.; Douillard, R. *J. Colloid Interface Sci.* **2007**, *316*, 388–397.
(27) Lee, K. H.; Kim, H. Y.; Khil, M. S.; Ra, Y. M.; Lee, D. R. *Polymer* **2003**, *44*, 1287–1294.
(28) Zhang, M.; Mueller, A. H. E. *J. Polym. Sci., Part A: Polym. Chem.* **2005**, *43*, 3461–3481.
(29) Beers, K. L.; Gaynor, S. G.; Matyjaszewski, K.; Sheiko, S. S.; Moeller, M. *Macromolecules* **1998**, *31*, 9413–9415.
(30) Belgacem, M. N.; Quillerou, J.; Gandini, A. *Eur. Polym. J.* **1993**, *29*, 1217–1224.
(31) Roman, M.; Winter, W. T. *Biomacromolecules* **2004**, *5*, 1671–1677.
(32) Dersch, R.; Graeser, M.; Greiner, A.; Wendorff, J. H. *Aust. J. Chem.* **2007**, *60*, 719–728.
(33) Huang, Z.-M.; Zhang, Y. Z.; Kotaki, M.; Ramakrishna, S. *Compos. Sci. Technol.* **2003**, *63*, 2223–2253.
(34) Favier, V.; Dendievel, R.; Canova, G.; Cavaille, J. Y.; Gilormini, P. *Acta Mater.* **1997**, *45*, 1557–1565.
(35) Habibi, Y.; Dufresne, A. *Biomacromolecules* **2008**, *9*, 1974–1980.
(36) Habibi, Y.; Goffin, A.-L.; Schiltz, N.; Duquesne, E.; Dubois, P.; Dufresne, A. *J. Mater. Chem.* **2008**, *18*, 5002–5010.
(37) Wang, M.; Jin, H. J.; Kaplan, D. J.; Rutledge, G. C. *Macromolecules* **2004**, *37*, 6856–6864.

AM9003705